Dose-Dependent Growth Delay of Breast Cancer Xenografts in the Bone Marrow of Mice Treated with ^{223}Ra: The Role of Bystander Effects and Their Potential for Therapy

Calvin N. Leung[1], Brian S. Canter[1,2], Didier Rajon[3], Tom A. Bäck[4], J. Christopher Fritton[2], Edouard I. Azzam[1], and Roger W. Howell[1]

[1]Department of Radiology, New Jersey Medical School, Rutgers University, Newark, New Jersey; [2]Department of Orthopedics, New Jersey Medical School, Rutgers University, Newark, New Jersey; [3]Department of Neurosurgery, University of Florida, Gainesville, Florida; and [4]Department of Radiation Physics, Sahlgrenska Academy, University of Gothenburg, Gothenburg, Sweden

The role of radiation-induced bystander effects in radiation therapy remains unclear. With renewed interest in therapy with α-particle emitters, and their potential for sterilizing disseminated tumor cells (DTCs), it is critical to determine the contribution of bystander effects to the overall response so they can be leveraged for maximum clinical benefit. **Methods:** Female *Foxn1$_{nu}$* athymic nude mice were administered 0, 50, or 600 kBq/kg $^{223}RaCl_2$ to create bystander conditions. At 24 hours after administration, MDA-MB-231 or MCF-7 human breast cancer cells expressing luciferase were injected into the tibial marrow compartment. Tumor burden was tracked weekly via bioluminescence. **Results:** The MDA-MB-231 xenografts were observed to have a 10-day growth delay in the 600 kBq/kg treatment group only. In contrast, MCF-7 cells had 7- and 65-day growth delays in the 50 and 600 kBq/kg groups, respectively. Histologic imaging of the tibial marrow compartment, α-camera imaging, and Monte Carlo dosimetry modeling revealed DTCs both within and beyond the range of the α-particles emitted from ^{223}Ra in bone for both MCF-7 and MDA-MB-231 cells. **Conclusion:** Taken together, these results support the participation of ^{223}Ra-induced antiproliferative/cytotoxic bystander effects in delayed growth of DTC xenografts. They indicate that the delay depends on the injected activity and therefore is dose-dependent. They suggest using $^{223}RaCl_2$ as an adjuvant treatment for select patients at early stages of breast cancer.

Key Words: α-particle; irradiation; bystander effect; breast cancer; ^{223}Ra

J Nucl Med 2020; 61:89–95
DOI: 10.2967/jnumed.119.227835

There has been renewed interest in radiopharmaceutical therapy since the U.S. Food and Drug Administration approved Xofigo (Cardinal Health, $^{223}RaCl_2$), an α-particle–emitting radiopharmaceutical, for palliative treatment of metastatic castration-resistant prostate cancer. Patients given $^{223}RaCl_2$ demonstrated decreases in bone pain and, unlike previous bone-metastatic palliative radiotherapies such as the β-emitting ^{89}Sr, increased survival (*1*). To understand these responses and guide clinical use of $^{223}RaCl_2$, detailed studies on its pharmacokinetics and dosimetry have been conducted (*2–6*). In addition, its clinical benefits have initiated other trials investigating the efficacy of $^{223}RaCl_2$ against other bone-metastatic cancers, such as breast cancer.

Breast cancer is the most common cancer diagnosed in women (*7*). A difficulty in successfully treating this cancer is the prevention and treatment of metastatic disease, with approximately 20% of 5-year survivors ultimately relapsing 5–10 years after treatment (*8*). The formation of metastases involves circulating tumor cells shedding from the primary tumor and gaining access to the circulatory system (*9*). Although most circulating tumor cells are rapidly eliminated, a small number survive and disseminate to various niches. These disseminated tumor cells (DTCs) may sustain active proliferation and develop into macrometastases or may remain dormant for years before becoming active. Using animal models, it was estimated that 2.5% of shed circulating tumor cells survive to become DTCs and approximately 0.01% may progress to macrometastases (*10*). Although the overall breast cancer 5-year survival rate is about 89%, patients with bone-metastatic tumors had a median survival of only 19–25 months from diagnosis (*11*). In one third of patients with stage I–III breast cancer, DTCs were found in bone marrow biopsies (*12*). Yet, despite the standard use of adjuvant therapy to address the issue of DTCs, 20% of breast cancer patients experience relapse (*8*). Recent studies have found that DTCs can occur early in cancer development, in contrast to the concept that tumor metastasis occurs in late-stage cancer only (*13*). DTCs are a significant risk factor in reducing patients' life expectancy (*9,14*). Therefore, a key goal for radionuclide therapies of cancer is to develop strategies to sterilize DTCs before they become micrometastases in bone.

A benefit of using $^{223}RaCl_2$ for treatment of DTCs is the emission of several short-range high–linear-energy-transfer α-particles (Supplemental Table 1 (*15–17*); supplemental materials are available at http://jnm.snmjournals.org). In comparison to low–linear-energy-transfer radiation, only a few traversals across the cell nucleus are sufficient to cause cell death (*18*). This is due to the α-particle's ability to cause clustered DNA damage, including complex DNA double-strand breaks (*19*). In addition, its principal localization in bone and the short track length of the α-particles (<70 μm in water) allow for better sparing of bone marrow than is possible with competing therapeutics that emit β-particles with

Received Feb. 27, 2019; revision accepted Jun. 7, 2019.
For correspondence or reprints contact: Roger W. Howell, Division of Radiation Research, Department of Radiology, New Jersey Medical School, Cancer Institute of New Jersey, Cancer Center F1208, 205 S. Orange Ave., Newark, NJ 07103.
E-mail: rhowell@rutgers.edu
Published online Sep. 13, 2019.

ranges of up to a centimeter or more, depending on their energy (*3,20*). Combined with its calcium mimetic properties that allow for rapid and preferential uptake to osseous surfaces at marrow interfaces, $^{223}RaCl_2$ is an α-emitter therapy well suited to treat tumor cells within the bone microenvironment. However, because of the α-particles' short track length, it is unlikely that every DTC in bone marrow is traversed by an α-particle (Fig. 1), suggesting additional mechanisms of action for the observed clinical benefits of longer survival. Cancer cells outside the scope of the radiation field are known to be indirectly affected by bystander effects. DTCs beyond the range of the α-particles may suffer toxic effects due to signals propagated by α-particle–irradiated cells. These signals can be transmitted by secreted factors and direct intercellular communication (*21–24*). The bystander effect has been shown to affect cells 1 mm away from the cells directly hit by radiation, many times farther than the range of the α-particle (*25*). This suggests that the biologic effects of α-therapy may extend beyond the range of the α-particle. However, how bystander effects impact the therapeutic efficacy of α-therapy and whether they can be leveraged are unclear (*26*). Animal studies have been conducted to demonstrate the capacity of $^{223}RaCl_2$ to treat prostate cancer metastases at various stages of disease in both preventive and therapeutic capacities, but the mechanisms underlying its efficacy have not been explored (*27,28*). Therefore, using a mouse model of DTCs in bone, the present study was conducted to determine whether bystander effects play a role in $^{223}RaCl_2$ therapy and, if so, whether they can be leveraged to treat DTCs at early stages of disease.

MATERIALS AND METHODS

Tumor Cells and Animals

MCF-7-luc-F5 (estrogen receptor–positive) and MDA-MB-231-luc-D3H1 (estrogen receptor–negative, progesterone receptor–negative, human epidermal growth factor receptor 2–negative) human breast cancer cells were obtained from Caliper Life Sciences and cultured in Leibovitz L-15 medium (Sigma-Aldrich) supplemented with 2 mM L-glutamine (Gibco), 100 IU/mL penicillin, 100 μg/mL streptomycin (Corning), and 10% (v/v) fetal bovine serum (Gibco). Cells were grown in 175 cm^2 flasks and passaged weekly. The cell lines were authenticated by ATCC using short-tandem-repeat analysis. MDA-MB-231-luc-D3H1 had an 86% match to the ATCC cell line HTB-26 (MDA-MB-231), with the allelic loss at loci D7S820 and vWA. MCF-7-luc-F5 had a 100% match to the ATCC cell line HTB-22 (MCF-7), with 14 of 14 alleles matching.

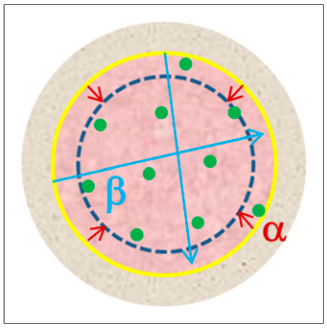

FIGURE 1. Depiction of marrow (pink) in bone (gray), comparing traversal lengths of β-particles (blue arrows) and α-particles (red arrows). ^{223}Ra is localized on bone surface (yellow). Cells within blue dotted circle are untouched by short-range α-particles. Range of β-particles varies because of their polyenergetic emission spectra.

Female *Foxn1^{nu}* athymic nude mice (4–6 weeks old, 18–23 g; Envigo) were housed in rectangular opaque M.I.C.E. cages (Animal Care Systems) in groups of 4 on wood shavings with no enrichment. Room temperature was 21°C–23°C with a 12-hour light/dark cycle. The mice were provided irradiated PicoLab Rodent Diet 20 (LabDiet) and water ad libitum. Moribund animals and those in apparent pain were euthanized with CO_2 followed by cervical dislocation. All procedures were approved by Rutgers Institutional Animal Care and Use Committee.

Creation of Bystander Conditions in Tibial Marrow Compartment

Measurement of Radioactivity in Hind Limbs. Previous data (*29*) suggested that the marrow compartment is largely free of ^{223}Ra and daughters by 24 hours after injection and is therefore a suitable location at that time for studies of radiation-induced bystander effects (Fig. 1). This was confirmed as follows. First, mice were administered 200 μL of 5 mM citrate-buffered saline containing 600 or 1,200 kBq/kg $^{223}RaCl_2$ via tail vein injection at 4:00–6:00 PM. At 24 or 48 hours after injection, the mice were euthanized by CO_2 asphyxiation. The tibiae and femurs were resected, and the activity in each was measured with a Packard Cobra automatic γ-counter for 2 min. Calibration (disintegrations per second = counts per minute/51.1) was conducted with an aliquot from a known concentration of clinical-grade $^{223}RaCl_2$. The resected tibiae were then processed to ascertain activity in cortical bone versus marrow. The tibial epiphyses were cut off, and the low-level activity in the cortical bone shaft was determined with a calibrated low-background high-purity germanium well counter (Canberra) using the 154.2-keV photopeak of ^{223}Ra (yield, 0.057; efficiency, 0.47). The bone marrow was purged from the diaphysis with 1 mL of phosphate-buffered saline using a 1-mL syringe with a 1.27-cm 27-gauge needle. Air was blown through the diaphyseal shaft, followed by centrifugation at 600*g* for 10 min to ensure all the flush was purged. Activity in the marrow and the flushed shaft was then measured and the percentage activity in marrow determined.

α-Imaging of Activity Distribution in Tibia. To determine the detailed spatial distribution of ^{223}Ra and daughter decays within the tibial and femoral bone and marrow, mice were administered $^{223}RaCl_2$ as above. At 72 hours after injection, the mice were euthanized and their hind limbs placed in ethanol. The limbs were then frozen in cryoprotective gel using liquid nitrogen-cooled isopentane, cryosectioned (12-μm thick) using a tape-transfer method (CryoJane; Leica), and imaged using an α-camera as described elsewhere (*30*). For each α-image section, a consecutive section was made, stained with hematoxylin and eosin, and used for morphologic identification.

Effective Clearance Half-Time. To determine the effective half-time T_e in the tibia for radiation dosimetry, mice were administered 600 kBq/kg $^{223}RaCl_2$ and then euthanized 1, 8, and 21 days after injection, after which tibial activity was measured. The T_e was determined by fitting data (SigmaPlot13; Systat Software, Inc.) to $A(t) = A_o\ e^{-0.693t/T_e}$.

Inoculation of Tumor Cells into Tibial Marrow Compartment

The breast cancer cells maintained in culture as adherent monolayers were used in experiments when 80%–90% confluent. They were detached by trypsinization and their concentration determined with a model ZM Coulter counter. Cells were pelleted at 2,000 rpm for 3 min in 14-mL centrifuge tubes; the medium was discarded, leaving a concentrated slurry of cells that was placed on ice. The mice were anesthetized with 2% isoflurane in O_2, and a 29-gauge insulin syringe was used to drill a hole into the tibial marrow compartment via a transpatellar approach. A chilled 31-gauge 10-μL Neuros syringe (Hamilton) loaded with 10^6 MDA-MB-231 cells or 4×10^5 MCF-7 cells in a 3-μL volume was inserted through the hole, and the cells were inoculated into the tibial marrow compartment. The larger size of the MCF-7 cells led to fewer cells in the 3-μL slurry. At 24 hours after xenografting, the mice were anesthetized with 2% isoflurane and injected subcutaneously with 200 μL of 15 mg/mL luciferin. To confirm successful inoculation and to determine initial bioluminescence intensity, serial images (IVIS 200, Perkin Elmer) were taken until maximum bioluminescence intensity was observed.

Measurement of Tumor Cell Proliferation

To examine whether bystander effects modulate proliferation or killing of DTCs in vivo, the $^{223}RaCl_2$ must be administered before

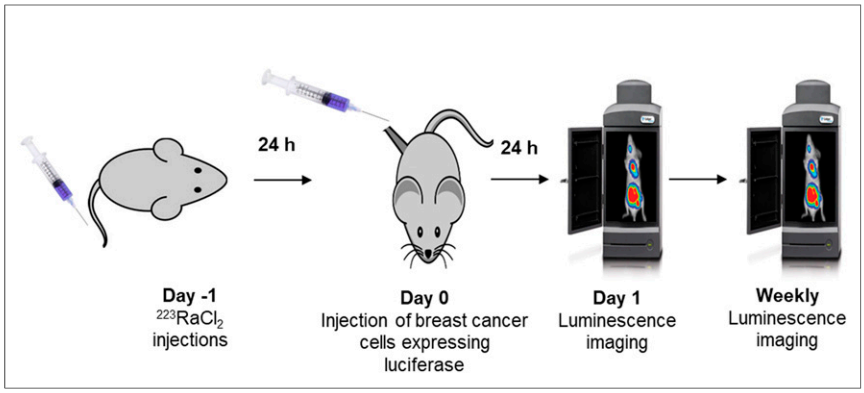

FIGURE 2. In vivo experimental timeline for measuring proliferation of DTCs. Animals were administered $^{223}RaCl_2$ intravenously on day −1. Breast cancer cells were administered on day 0. Luminescence imaging was conducted on day 1 and then weekly.

tumor cell inoculation and the inoculation must take place after the circulating ^{223}Ra clears. Accordingly, the mice were injected with 0, 50, or 600 kBq/kg $^{223}RaCl_2$ on day −1, followed by intratibial inoculation of cells on day 0 (Fig. 2). On day 1 and weekly thereafter, the bioluminescence intensity was measured with IVIS. The normalized bioluminescence intensity was taken as the ratio of the average luminescence intensities in test and control groups. A 2-way ANOVA with post hoc Bonferroni comparison determined significance ($P < 0.05$) between treatment groups.

Spatial Location of Tumor Cells in Tibial Marrow Compartment

Mice were treated with 0 or 600 kBq/kg $^{223}RaCl_2$ on day −1. On day 0, 80%–90% confluent breast cancer cells were washed twice with phosphate-buffered saline, which had been labeled with 10 mL of 1-μM CellTracker Green (Thermo Fisher) in unsupplemented L-15 medium for 45 min. The cells were then trypsinized and inoculated intratibially. IVIS on days 1 and 3 confirmed successful inoculation. Following detection of luminescence signal, the mice were euthanized and the tibiae resected. The resected tibiae were imaged with IVIS to confirm that the previous signal observed was within the tibial marrow compartment. The tibiae were placed in 7 mL of 4% paraformaldehyde and fixed for 48 hours at 4°C. Samples were then decalcified in 14% ethylenediaminetetraacetic acid for 2 weeks, followed by paraffin embedment. Transverse sections (5-μm thick) were cut with a microtome and stained with hematoxylin and eosin. A Nikon A1R confocal microscope was used to image the fluorescence (517-nm peak) emitted by the CellTracker Green labeled breast cancer cells.

Absorbed Dose Profile in Tibial Bone and Marrow

A section of a mouse tibia was modeled using the Monte Carlo simulation toolkit Geant4 (*31*). First, a series of small-animal CT images of a mouse tibia was acquired (Bruker Skyscan 1172) with a 5.0-μm voxel size. Second, the images were processed to extract the endosteal and periosteal surfaces, which were then converted into tessellated solids suitable for transport by Geant4. Third, the marrow and cortical bone compartments where subdivided into 2.0-μm layers from the endosteal surface. Details regarding the software and parameters are provided in Supplemental Table 2.

Five million ^{223}Ra decays and ensuing daughter decays were simulated in a 400-μm-long transverse section of the tibial diaphysis. Because redistribution of the daughters is less than 1% (*29*), daughter decays were simulated at the ^{223}Ra parent decay sites. The emitted radiations were transported with Geant4, and energy depositions were scored in a 1,600-μm-long region surrounding the decay region. On the basis of the activity measurements reported in this article, 99.2% of decays were in the cortical bone and only 0.8% in the marrow cavity. Exponential distributions based on α-camera activity quantitation were used to concentrate decays along the bone surface with a half-thickness of 75.0 μm within the bone tissue and 37.0 μm within the marrow tissue. The International Commission on Radiological Protection tissue composition for cortical bone and soft tissue were used for the bone and marrow compartments, respectively (*32*).

RESULTS

Measurement of Radioactivity in Hind Limbs

Measurements of femoral ^{223}Ra activity yielded no significant difference in counts between femurs harvested at 24 hours after injection of $^{223}RaCl_2$ and those harvested at 48 hours (Supplemental Fig. 1). This finding is in agreement with published data for mice (*29,33*). Therefore, it was concluded that maximum bone uptake was achieved by 24 hours after injection, supporting the selection of this time to inoculate the tibia with breast cancer cells. Uptake of ^{223}Ra in the hind limbs at 24 hours was linearly dependent on the injected activity (Supplemental Fig. 2). Measurements of tibial activity with the high-purity germanium detector determined that the epiphyses, diaphysis, and bone marrow contained 63.0% ± 3.1%, 36.7% ± 3.4%, and 0.30% ± 0.12% of the total tibial activity, respectively, and that diaphyseal bone marrow contained 0.80% ± 0.73% of the activity in the diaphysis (Supplemental Fig. 3).

α-imaging of tibiae showed that ^{223}Ra was concentrated to bone surfaces and active growth locations, particularly in the proximal epiphysis (Figs. 3A and 3B). Quantification by digital postprocessing showed that the emitted α-particles are detected predominantly in bone, with very few events (2.1% ± 1.3%) in marrow (Fig. 3C). This percentage is similar to the 0.80% ± 0.73% obtained with the high-purity germanium measurements. The high-purity germanium–derived value is used for dosimetry calculations because it represents

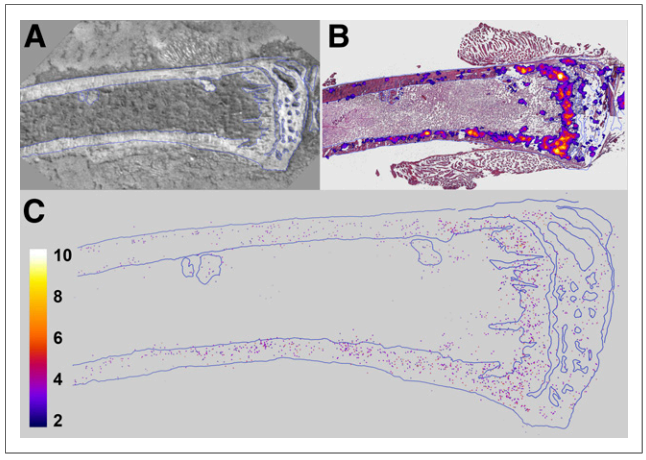

FIGURE 3. Images of longitudinal section of mouse tibia harvested 24 hours after administration of 1,200 kBq of $^{223}RaCl_2$ per kilogram. (A) Bright-field image of unstained section. (B) Merge of bright-field image (hematoxylin- and eosin-stained) and low-resolution multiple-event α-camera image. (C) High-resolution single-event postprocessed α-camera image that identifies precise locations of α-particle events.

an average over the relevant portion of the marrow compartment. Finally, least-squares fits of the radial activity distribution to exponential functions yielded half-thicknesses of 75.0 and 37.0 μm in the diaphyseal bone and marrow, respectively (Supplemental Fig. 4).

Effective and Biologic Half-Lives of ^{223}Ra in Tibia

Using a least-squares fit of the data to a monoexponential decay function, the T_e of ^{223}Ra in the tibia and femur were 10.0 and 10.3 days, respectively (Supplemental Fig. 5). The biologic half-times were determined using $1/T_e = 1/T_p + 1/T_b$, where T_p and T_b represent the physical half-life and biologic half-time, respectively. The T_p for ^{223}Ra is 11.4 days, and the calculated T_b was 81 days and 107 days for the tibia and femur, respectively. These values indicate that the effective clearance of ^{223}Ra from the tibia is driven primarily by physical decay, with a small contribution from biologic clearance.

Tumor Cells in Marrow Lie Within and Beyond Range of α-Particles Emitted from Bone

Histologic sections of tibiae, harvested from both the 0 kBq/kg and the 600 kBq/kg treatment groups at 24 and 72 hours after inoculation, showed breast cancer cells within and beyond the 70-μm range of the α-particles (Fig. 4; Supplemental Figs. 6 and 7). Therefore, the in vivo model contains breast cancer cells that will be directly irradiated by the α-particles, as well as a bystander population of breast cancer cells farther from the bone endosteum and unlikely to be traversed by an α-particle.

Absorbed Dose Profile in Tibial Bone and Marrow

The small-animal CT–derived tessellated solids representing the tibia, and the absorbed dose distribution obtained with the Geant4 Monte Carlo simulation of 5×10^6 decays, are presented in Figure 5. The total absorbed doses (absorbed dose from alpha particles, absorbed dose from beta particles) in the bone and marrow compartments were 37.0 Gy (D_α = 36.4 Gy, D_β = 0.77 Gy) and 2.59 Gy (D_α = 2.36 Gy, D_β = 0.23 Gy), respectively, for 5×10^6 decays, with a statistical error of less than 0.1%. Inside the marrow cavity, the dose is concentrated within 70 μm of the endosteum, which corresponds to the maximum range of the α-particles emitted from ^{223}Ra and daughter decays in the bone. In the bystander region, the

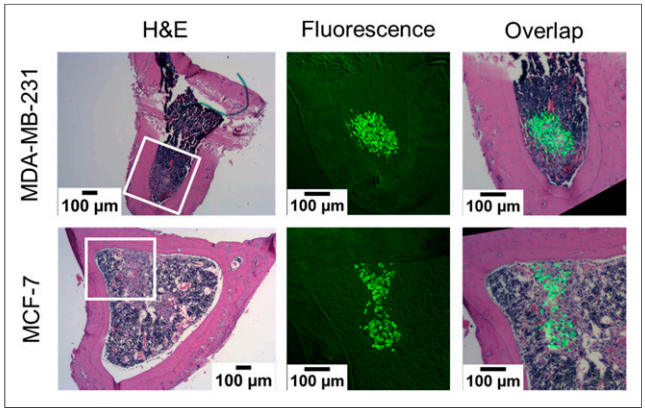

FIGURE 4. Histologic images of transverse sections of mouse tibiae that were harvested 24 hours after inoculation with CellTracker Green labeled MDA-MB-231 or MCF-7 breast cancer cells. Shown are bright-field hematoxylin and eosin (H&E) and green fluorescence images of adjacent sections. Tumor cells are present within and beyond 70-μm range of α-particles emitted from bone surfaces. Additional tibial sections are shown in Supplemental Figures 6 and 7 (600 kBq/kg, 24 hours after inoculation, and 0 and 600 kBq/kg, 72 hours after inoculation, respectively).

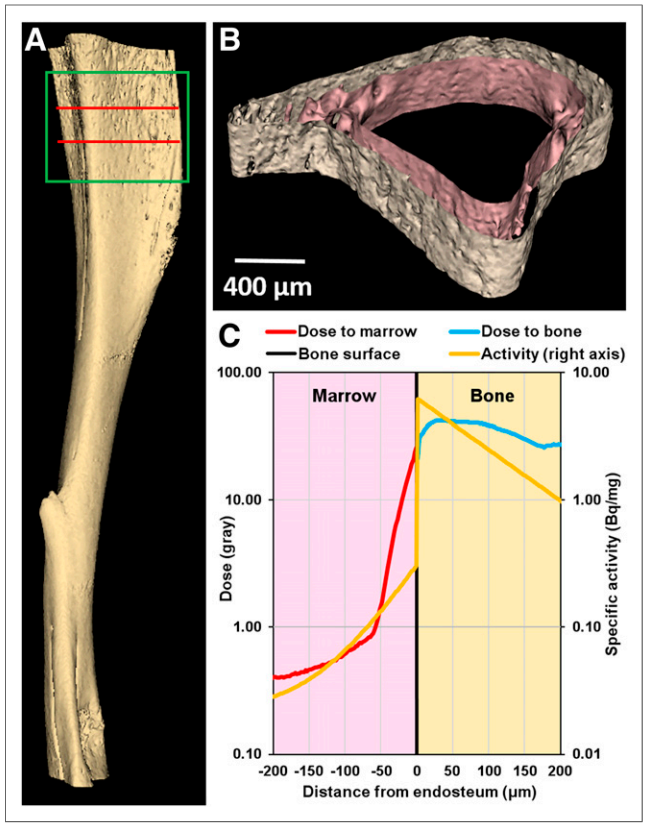

FIGURE 5. (A) Three-dimensional model of mouse tibia reconstructed from small-animal CT images. Section used for Monte-Carlo simulation corresponds to green box. Radioactivity was restricted to 400-μm-thick section delineated by 2 red lines: bone volume = 0.27 mm^3, bone mass = 0.52 mg, marrow volume = 0.39 mm^3, marrow mass = 0.40 mg. (B) Transverse cross section of 400-μm-thick region showing surfaces of endosteum and periosteum. (C) Absorbed dose distribution in marrow cavity (red curve) and cortical bone (blue curve) vs. distance from endosteum after 5×10^6 ^{223}Ra decays and ensuing daughter decays. Yellow curve shows activity distribution based on analysis of α-camera data (Supplemental Fig. 4).

α-particles emitted by the few decays that occur in the marrow cavity, and the β-particles emitted by ^{223}Ra daughters in the bone compartment, contribute to an absorbed dose of less than 0.8 Gy (D_α = 0.56 Gy, D_β = 0.27 Gy). The 5×10^6 decays correspond to complete decay of an initial activity of 4.0 Bq of ^{223}Ra in the modeled 400-μm region. However, the measured activity corresponding to the modeled 400-μm region was 2.3 Bq for the 600 kBq/kg administration. Therefore, given these activities, and the linear uptake depicted in Supplemental Fig. 2, the mean absorbed dose per unit injected activity to diaphyseal bone and marrow was 3.5×10^{-2} Gy (kBq/kg)$^{-1}$ and 2.4×10^{-3} Gy (kBq/kg)$^{-1}$, respectively. The absorbed dose to the bystander region ranged from 3.8×10^{-4} Gy (kBq/kg)$^{-1}$ to 7.7×10^{-4} Gy (kBq/kg)$^{-1}$. Absorbed doses for the different injected activities, and initial dose rates [$r_o = D(t=\infty)/(1.44\ T_e)$] to the bystander region, are summarized in Table 1.

Tumor Cell Proliferation

Tumor burden is given as normalized bioluminescence intensity in Figure 6. The growth delays for each treatment group, defined by Demidenko as the difference of times required for treated and untreated tumors to double their initial size (*34*), are given in Table 1. The MDA-MB-231 cells demonstrated a modest delay in tumor progression for the 600 kBq/kg group ($P < 0.001$), and no significant

TABLE 1
Growth Delay of Human Breast Cancer Xenografts

$^{223}RaCl_2$ treatment (kBq/kg)	D_{bone} (Gy)*	D_{marrow} (Gy)*	$D_{bystander}$ (Gy)*	$r_{o,bystander}$ (Gy/h)†	Doubling time (days)		Growth delay (days)	
					MCF-7	MDA-MB-231	MCF-7	MDA-MB-231
0	0	0	0	0	20	23	0	0
50	D_α = 1.74	D_α = 0.11	D_α = 0.01–0.03	$0.58–1.2 \times 10^{-4}$	27	9.4	7	−14
	D_β = 0.04	D_β = 0.01	D_β = 0.01–0.013					
	D_{tot} = 1.8	D_{tot} = 0.12	D_{tot} = 0.02–0.04					
600	D_α = 20.9	D_α = 1.36	D_α = 0.12–0.32	$0.67–1.3 \times 10^{-3}$	86	33	65	10
	D_β = 0.44	D_β = 0.13	D_β = 0.11–0.16					
	D_{tot} = 21	D_{tot} = 1.5	D_{tot} = 0.23–0.48					

*Absorbed dose for complete decay (integrated to $t = \infty$).
†Initial dose rate r_o to bystander compartment.
D_α = absorbed dose from alpha particles; D_β = absorbed dose from beta particles; $D_{tot} = D_\alpha + D_\beta$.
Doubling time and growth delay are as defined by Demidenko (*34*).

difference for the 50 kBq/kg group, when compared with control. MCF-7 cells appeared to respond to both the 50 kBq/kg ($P = 0.09$) and the 600 kBq/kg ($P < 0.001$) treatment; only the 600 kBq/kg treatment was significant. The MCF-7 600 kBq/kg group showed a marked decrease in tumor burden of approximately 70% that was not observed in other groups (Fig. 6). In all treated groups, exponential tumor growth rate (normalized bioluminescence intensity = $a\,e^{bt}$) returned eventually to that of control (MCF-7: b = 0.053 ± 0.011, 0.064 ± 0.021, and 0.052 ± 0.031 $days^{-1}$ for 0, 50, and 600 kBq/kg; MDA-MB-231: b = 0.080 ± 0.003, 0.149 ± 0.029, and 0.103 ± 0.007 $days^{-1}$).

DISCUSSION

The tumor progression studies in Figure 6 show that MDA-MB-231 and MCF-7 responded very differently when placed into a marrow compartment that is surrounded by an in vivo α-particle irradiator formed by the ^{223}Ra in the bone. In the presence of ^{223}Ra, proliferation was curtailed more robustly for MCF-7 cells than MDA-MB-231 cells at both the low (50 kBq/kg) and the high (600 kBq/kg) injected activities (Table 1). Given that tumor cells are found both near and far from the bone surface relative to the range of the α-particles, this result could simply be a consequence of differences in absorbed doses received by the cells or differences in sensitivity to direct irradiation or induced bystander effects.

There are several factors arguing against either location or sensitivity to direct irradiation as being a primary contributor. First, the distribution of tumor cells in the tibial marrow compartment is similar for both MCF-7 and MDA-MB-231 (Fig. 4; Supplemental Figs. 6–7). Thus, they were exposed to the same absorbed dose profiles (Fig. 5). Second, the maximum mean absorbed dose delivered to the bystander region by α-particles is 0.32 Gy for complete decay of the 600 kBq/kg administration (Table 1). According to Charlton et al. (*35*), this will result in only about 20% of the cell nuclei being hit (any chord length) by an α-particle after 10 days, 30% in 20 days, and 40% for complete decay (Fig. 7 of Charlton et al.). Third, extensive studies with these 2 cell lines, wherein responses to ionizing radiation were examined in parallel under well-controlled conditions, demonstrated similar sensitivities to high–dose-rate exposures as evidenced by clonogenic cell survival (*36–38*). Fourth, MCF-7 cells do not demonstrate low-dose hypersensitivity (*39*), and their radioresistance is increased at low–dose-rate exposures (*40*). Taken together, these points suggest that the different responses of these 2 cell lines are likely due to different sensitivities to radiation-induced stressful bystander effects that cause decreased proliferation or cell death (Fig. 6). These findings are supported by our published

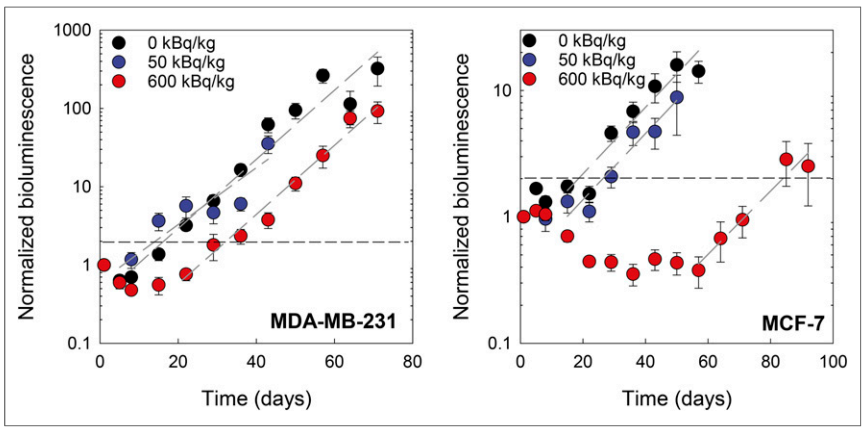

FIGURE 6. Tumor burden, measured with luminescence imaging, of MDA-MB-231 (left) and MCF-7 (right) cells under bystander conditions induced by radiation in vivo. Cells were inoculated into mouse tibiae 1 day after administration of 0, 50, or 600 kBq of $^{223}RaCl_2$ per kilogram. Values are given as average ($n = 6$) ± SEM. Black horizontal dashed line delineates 2-fold increase in initial normalized luminescence intensity. Dashed gray lines are exponential least-squares fits to terminal data points for each dataset. Representative luminescence images of tumor burden in 0 and 600 kBq/kg treatment groups at various times after inoculation are shown in Supplemental Figures 8 and 9, respectively.

in vitro studies showing that high–linear-energy-transfer radiation-induced lethal bystander effects are more robust for MCF-7 than for MDA-MB-231 (*41*), as well as by the antiproliferative bystander effect observed in vivo by Xue et al. (*42*).

The shape of the tumor response curves in Figure 6 and the growth delays reported in Table 1 support a bystander response that depends on dose and dose rate. The dose rate decrease half-time is equal to the effective clearance half-time of ^{223}Ra from the tibia, which is 10 days (Supplemental Fig. 5). The nadir of MCF-7 tumor burden occurs at 40 days for 600 kBq/kg, at which time dose rate has dropped about 16-fold and the rate of reduction in tumor burden begins to diminish. The dose rate produced by a 600 kBq/kg injection at this time (40 days) is about the same as produced by 50 kBq/kg at 0 days, and their effect on tumor burden is similar, suggesting that an injected-activity–dependent bystander effect occurred within the bone microenvironment that affects both tumor cell burden and growth, depending on breast cancer phenotype.

Strictly, no single definition fits the type of bystander conditions that are present in ^{223}Ra therapy because of its nonuniform activity distribution and complex mixture of emitted radiations (α, β, γ, x). Bystander effects have been defined classically as responses of unirradiated cells to signals emanating from irradiated cells (*43*), and cohort effects have been defined as those responses that occur within an irradiated cell population not attributed to effects caused by direct radiation hits (*43,44*). Both can be transmitted via gap junctional intercellular communication or released factors and are thus not attributed to the radiation hits directly. Abscopal effects arise in an entirely different locale that is distant from the region irradiated (*43*). Here, all 3 classes of effects are possible, tempting attribution of the observed responses as "nontargeted" in the sense that radiation hits are not directly responsible for some of the observed effect. Although *nontargeted* is a widely used term in external-beam radiobiology, the use of the term *targeted* in nuclear medicine refers to localization of the radiopharmaceutical to a specific population of cells or treatment region. Therefore, the use of the phrase *nontargeted effects* is inappropriate in this context, and we simply call the effect observed in the present work a bystander effect in the sense that irradiated cells (e.g., tumor cells, marrow constituents, osteocytes, and osteoblasts in the skeleton) are responsible for imparting effects to tumor cells in the marrow compartment that may or may not have been irradiated. This terminology is consistent with clinical implementation of radiopharmaceutical therapy, in which cells are irradiated while the radiopharmaceutical circulates throughout the body and concentrates in the tumor, making it unlikely that there are cells in the marrow that are not irradiated at all. Key to this and recognized by both Blyth and Sykes (*43*) and Brady et al. (*26*) is the understanding that a bystander is a cell that may have been either irradiated or unirradiated and a bystander effect is one imparted from irradiated cells. With the recent shift in targeted, high–linear-energy-transfer radiotherapy, being able to kill bystanders will be highly beneficial in the design of future treatment plans for radiopharmaceuticals alone or combined with external-beam therapy.

The increased magnitude of the bystander effect in the present study suggests that higher injected activities may better sterilize undetected dormant or slow-growing DTCs in the bone marrow microenvironment. Thus, $^{223}RaCl_2$ may be a potential adjuvant therapy. Indeed, past studies suggest that there may be some benefit to escalating injected activity when treating advanced stages of disease (*45*). Although $^{223}RaCl_2$ is currently approved at 50 kBq/kg, tolerance has been demonstrated at activities of as high as 200 kBq/kg per injection in patients and higher amounts have not been explored (*6*). Although a single treatment of $^{223}RaCl_2$ in the current study was insufficient to sterilize all DTCs in the bone marrow, multiple treatments may yield a more durable tumor response. Additionally, the different in vivo responses of the MCF-7 and MDA-MB-231 cells suggests that some patient subsets with breast cancer DTCs may derive greater benefit from $^{223}RaCl_2$ therapy than other patient subsets (*41*). Characterization of the DTCs within the bone marrow may be required to determine which patients are likely to benefit most from $^{223}RaCl_2$ therapy. Further work is required to determine the molecular mechanisms by which bystander cells are killed or inhibited in growth and which DTC phenotypes would likely benefit from early $^{223}RaCl_2$ administration. Given the difference in responses of the MCF-7-*luc*-F5 (estrogen receptor–positive) and MDA-MB-231-*luc*-D3H1 (estrogen receptor–negative, progesterone receptor–negative, human epidermal growth factor receptor 2–negative) human breast cancer cells to bystander signals elicited by $^{223}RaCl_2$, and the success of $^{223}RaCl_2$ against metastatic castration-resistant prostate cancer (*1*), the potential for leveraging these bystander effects should be further explored experimentally and clinically in the context of hormone-related cancers.

CONCLUSION

Taken together, the data indicate that radiation-induced bystander effects play an important role in the response of some DTCs to $^{223}RaCl_2$ and that the response depends on injected activity. These results support the use of $^{223}RaCl_2$ as an adjuvant treatment for select patients at early stages of breast cancer.

DISCLOSURE

This study was supported in part by grant 1R01CA198073 from the NIH and by New Jersey Commission on Cancer Research predoctoral fellowship grants DFHS15PPC009 (Calvin Leung) and DFHS17PPC029 (Brian Canter). No other potential conflict of interest relevant to this article was reported.

ACKNOWLEDGMENTS

We thank Patricia Buckendahl and the Rutgers Molecular Imaging Center for small-animal CT imaging.

KEY POINTS

QUESTION: Can radiation-induced bystander effects, produced by ^{223}Ra, be used to treat DTCs in bone marrow?

PERTINENT FINDINGS: ^{223}Ra-induced bystander effects contribute to significant growth delays of human breast cancer xenografts in the bone marrow of nude mice. The magnitude of the effect depends on dose and the breast cancer xenograft.

IMPLICATIONS FOR PATIENT CARE: The results suggest using $^{223}RaCl_2$ as an adjuvant treatment for select patients at early stages of breast cancer.

REFERENCES

1. Parker C, Nilsson S, Heinrich D, et al. Alpha emitter radium-223 and survival in metastatic prostate cancer. *N Engl J Med.* 2013;369:213–223.
2. Chittenden SJ, Hindorf C, Parker CC, et al. A phase 1, open-label study of the biodistribution, pharmacokinetics, and dosimetry of ^{223}Ra-dichloride in patients with hormone-refractory prostate cancer and skeletal metastases. *J Nucl Med.* 2015;56:1304–1309.

3. Hobbs RF, Song H, Watchman CJ, et al. A bone marrow toxicity model for ^{223}Ra alpha-emitter radiopharmaceutical therapy. *Phys Med Biol.* 2012;57:3207–3222.
4. Lassmann M, Nosske D. Dosimetry of ^{223}Ra-chloride: dose to normal organs and tissues. *Eur J Nucl Med Mol Imaging.* 2013;40:207–212.
5. Pratt BE, Hindorf C, Chittenden SJ, Parker CC, Flux GD. Excretion and whole-body retention of radium-223 dichloride administered for the treatment of bone metastases from castration resistant prostate cancer. *Nucl Med Commun.* 2018; 39:125–130.
6. Carrasquillo JA, O'Donoghue JA, Pandit-Taskar N, et al. Phase I pharmacokinetic and biodistribution study with escalating doses of ^{223}Ra-dichloride in men with castration-resistant metastatic prostate cancer. *Eur J Nucl Med Mol Imaging.* 2013;40:1384–1393.
7. Cancer stat facts: female breast cancer. NIH website. https://seer.cancer.gov/statfacts/html/breast.html. Accessed September 25, 2019.
8. Brewster AM, Hortobagyi GN, Broglio KR, et al. Residual risk of breast cancer recurrence 5 years after adjuvant therapy. *J Natl Cancer Inst.* 2008;100:1179–1183.
9. Wan L, Pantel K, Kang Y. Tumor metastasis: moving new biological insights into the clinic. *Nat Med.* 2013;19:1450–1464.
10. Tachtsidis A, McInnes LM, Jacobsen N, Thompson EW, Saunders CM. Minimal residual disease in breast cancer: an overview of circulating and disseminated tumour cells. *Clin Exp Metastasis.* 2016;33:521–550.
11. Selvaggi G, Scagliotti GV. Management of bone metastases in cancer: a review. *Crit Rev Oncol Hematol.* 2005;56:365–378.
12. Braun S, Vogl FD, Naume B, et al. A pooled analysis of bone marrow micrometastasis in breast cancer. *N Engl J Med.* 2005;353:793–802.
13. Hüsemann Y, Geigl JB, Schubert F, et al. Systemic spread is an early step in breast cancer. *Cancer Cell.* 2008;13:58–68.
14. Hayashi N, Yamauchi H. Role of circulating tumor cells and disseminated tumor cells in primary breast cancer. *Breast Cancer.* 2012;19:110–117.
15. Eckerman KF, Endo A. *MIRD: Radionuclide Data and Decay Schemes.* 2nd ed. Reston, VA: Society of Nuclear Medicine; 2008.
16. *Stopping Powers for Electrons and Positrons.* Bethesda, MD: International Commission on Radiation Units and Measurements; 1984. ICRU report 37.
17. *Stopping Powers and Ranges for Protons and Alpha Particles.* Bethesda, MD: International Commission on Radiation Units and Measurements; 1993.
18. Howell RW, Narra VR, Rao DV, Sastry KSR. Radiobiological effects of intracellular polonium-210 alpha emissions: a comparison with auger-emitters. *Radiat Prot Dosimetry.* 1990;31:325–328.
19. Goodhead DT. Initial events in the cellular effects of ionizing radiations: clustered damage in DNA. *Int J Radiat Biol.* 1994;65:7–17.
20. Bouchet LG, Bolch WE, Goddu SM, Howell RW, Rao DV. Considerations in the selection of radiopharmaceuticals for palliation of bone pain from metastatic osseous lesions. *J Nucl Med.* 2000;41:682–687.
21. Azzam EI, de Toledo SM, Little JB. Direct evidence for the participation of gap-junction mediated intercellular communication in the transmission of damage signals from alpha-particle irradiated to non-irradiated cells. *Proc Natl Acad Sci USA.* 2001;98:473–478.
22. Gaillard S, Pusset D, de Toledo SM, Fromm M, Azzam EI. Propagation distance of the alpha-particle-induced bystander effect: the role of nuclear traversal and gap junction communication. *Radiat Res.* 2009;171:513–520.
23. Bishayee A, Rao DV, Howell RW. Evidence for pronounced bystander effects caused by nonuniform distributions of radioactivity using a novel three-dimensional tissue culture model. *Radiat Res.* 1999;152:88–97.
24. Mothersill C, Seymour C. Medium from irradiated human epithelial cells but not human fibroblasts reduces the clonogenic survival of unirradiated cells. *Int J Radiat Biol.* 1997;71:421–427.
25. Belyakov OV, Mitchell SA, Parikh D, et al. Biological effects in unirradiated human tissue induced by radiation damage up to 1 mm away. *Proc Natl Acad Sci USA.* 2005;102:14203–14208.
26. Brady D, O'Sullivan JM, Prise KM. What is the role of the bystander response in radionuclide therapies? *Front Oncol.* 2013;3:215.
27. Suominen MI, Rissanen JP, Kakonen R, et al. Survival benefit with radium-223 dichloride in a mouse model of breast cancer bone metastasis. *J Natl Cancer Inst.* 2013;105:908–916.
28. Henriksen G, Breistol K, Bruland OS, Fodstad O, Larsen RH. Significant antitumor effect from bone-seeking, alpha-particle-emitting ^{223}Ra demonstrated in an experimental skeletal metastases model. *Cancer Res.* 2002;62:3120–3125.
29. Henriksen G, Fisher DR, Roeske JC, Bruland OS, Larsen RH. Targeting of osseous sites with alpha-emitting ^{223}Ra: comparison with the beta-emitter ^{89}Sr in mice. *J Nucl Med.* 2003;44:252–259.
30. Chouin N, Lindegren S, Frost SH, et al. Ex vivo activity quantification in micrometastases at the cellular scale using the alpha-camera technique. *J Nucl Med.* 2013;54:1347–1353.
31. Agostinelli S, Allison J, Amako K, et al. Geant4: a simulation toolkit. *Nucl Instrum Methods Phys Res A.* 2003;A506:250–303.
32. International Commission on Radiological Protection. *Basic Anatomical and Physiological Data for Use in Radiological Protection: The Skeleton.* Oxford, U.K.: Pergamon Press; 1994. ICRP publication 70.
33. Abou DS, Ulmert D, Doucet M, Hobbs RF, Riddle RC, Thorek DL. Whole-body and microenvironmental localization of radium-223 in naive and mouse models of prostate cancer metastasis. *J Natl Cancer Inst.* 2015;108:djv380.
34. Demidenko E. Three endpoints of in vivo tumour radiobiology and their statistical estimation. *Int J Radiat Biol.* 2010;86:164–173.
35. Charlton DE, Utteridge TD, Allen BJ. Theoretical treatment of human haemopoietic stem cell survival following irradiation by alpha particles. *Int J Radiat Biol.* 1998;74:111–118.
36. Liu X, Sun C, Jin X, et al. Genistein enhances the radiosensitivity of breast cancer cells via G_2/M cell cycle arrest and apoptosis. *Molecules.* 2013;18:13200–13217.
37. Duangmano S, Sae-Lim P, Suksamrarn A, Patmasiriwat P, Domann FE. Cucurbitacin B causes increased radiation sensitivity of human breast cancer cells via G2/M cell cycle arrest. *J Oncol.* 2012;2012:601682.
38. Sun Q, Liu T, Yuan Y, et al. MiR-200c inhibits autophagy and enhances radiosensitivity in breast cancer cells by targeting UBQLN1. *Int J Cancer.* 2015;136: 1003–1012.
39. Enns L, Bogen KT, Wizniak J, Murtha AD, Weinfeld M. Low-dose radiation hypersensitivity is associated with p53-dependent apoptosis. *Mol Cancer Res.* 2004;2:557–566.
40. Niedbala M, McNamee JP, Raaphorst GP. Response to pulsed dose rate and low dose rate irradiation with and without mild hyperthermia using human breast carcinoma cell lines. *Int J Hyperthermia.* 2006;22:61–75.
41. Akudugu JM, Azzam EI, Howell RW. Induction of lethal bystander effects in human breast cancer cell cultures by DNA-incorporated iodine-125 depends on phenotype. *Int J Radiat Biol.* 2012;88:1028–1038.
42. Xue LY, Butler NJ, Makrigiorgos GM, Adelstein SJ, Kassis AI. Bystander effect produced by radiolabeled tumor cells in vivo. *Proc Natl Acad Sci USA.* 2002;99: 13765–13770.
43. Blyth BJ, Sykes PJ. Radiation-induced bystander effects: what are they, and how relevant are they to human radiation exposures? *Radiat Res.* 2011;176:139–157.
44. Autsavapromporn N, De Toledo SM, Buonanno M, Jay-Gerin JP, Harris AL, Azzam EI. Intercellular communication amplifies stressful effects in high-charge, high-energy (HZE) particle-irradiated human cells. *J Radiat Res (Tokyo).* 2011;52: 408–414.
45. Nilsson S, Strang P, Aksnes AK, et al. A randomized, dose-response, multicenter phase II study of radium-223 chloride for the palliation of painful bone metastases in patients with castration-resistant prostate cancer. *Eur J Cancer.* 2012; 48:678–686.